Monte Carlo Guiding-Centre Simulations of $E \times B$ Flow Shear in Edge Transport Barrier

T.P. Kiviniemi[(1)], J.A. Heikkinen[(2)], A.G. Peeters[(3)], S.K. Sipilä[(1)]

[(1)] *Helsinki University of Technology, Advanced Energy Systems, Euratom-TEKES Association, P.O. Box 2200, FIN-02015 HUT, Finland*

[(2)] *VTT Chemical Technology, Euratom-TEKES Association, P.O. Box 1404, FIN-02044 VTT, Finland*

[(3)] *Max-Planck-Institut für Plasmaphysik - EURATOM Association, D-85748 Garching, Germany*

Abstract. $E_r \times B$ flow shear is simulated with a fully kinetic five-dimensional neoclassical Monte Carlo simulation both for JET and ASDEX Upgrade. Here, E_r is the radial electric field and B is the magnetic field. It is shown that high enough shear for turbulence suppression can be driven at the Low (L) to High (H) transition conditions without taking into account anomalous processes in E_r shear formation. For typical plasma parameters, at certain edge temperature, shear is weaker in JET than in ASDEX Upgrade thus requiring higher edge temperature for L–H transition as observed also in experiments. However, although the simulation is done at experimentally observed L–H transition temperature of each device, shear is still weaker at JET which proposes that the critical shear at JET should be lower than in ASDEX Upgrade. Parametric dependence of the shear on temperature, density and magnetic field is investigated and the effects of density and temperature gradients, plasma current and the direction of the ∇B drift on the shear are discussed.

Short title: Monte Carlo Simulations of $E \times B$ Flow Shear

PACS: 52.25 Fi, 52.55 Fa, 52.65 Pp

1 Introduction

Flow shear, especially the shear in $E_r \times B$ rotation, has been shown to have a stabilising effect on plasma turbulence level both in theory [1] and in experiments [2]. This is assumed to be an explanation for the transport barriers observed at the plasma edge in many tokamaks [3]. Here, E_r is the radial electric field and B is the magnetic field. However, the birth mechanism of the shear is still unclear. In the L–H transition, the plasma jumps from a low (L) confinement mode into the high (H) confinement mode and the energy confinement time is significantly increased. The criterion for the critical shear for strong turbulence suppression already exists in analytic theory [4] and it has also been measured in experiments [5–7]. Different mechanisms proposed for the generation of E_r are reviewed in Refs. [3,8]. The effect of ion orbit losses on E_r and its possible bifurcation was first studied analytically without radial dimension in Ref. [9]. This work has been critizised since it has assumed that the main ion and impurity ion rotation are identical although they are shown to have opposite sign in experiments [10]. One-dimensional simulation of the shear in E_r has been performed using multi-fluid equations including also some turbulent effects [11,12]. All these numerical treatments are done in a circular geometry and many simplifications have been done in evaluating the ion orbit loss current. In Ref. [13], E_r was solved for the first time with a fully kinetic five-dimensional (three dimensions in configuration space and two velocity dimensions) neoclassical Monte Carlo simulation of the tokamak plasma edge in a realistic ASDEX (Axially Symmetric Divertor EXperiment) Upgrade divertor geometry, thus avoiding many of the assumptions made in earlier analytic and numerical fluid treatments. Especially, validity of the analysis is not limited to some special collisionality regime, thin orbit approximation is not needed, effect of radial electric field on ion orbits is correctly modelled also for high Mach numbers, and there is no need to make assumptions to separate different current components which consist of same current carriers, but they are consistently evaluated from the guiding-centre motion. In that paper, it was shown that high enough shear for turbulence suppression can be driven without taking into account anomalous processes in E_r shear formation. Here, as a continuation of that work, a similar simulation is done for the JET (Joint European Torus) plasma and the results are compared to the earlier ASDEX Upgrade simulations. The possible effect of gradients in density and temperature, as well as the effect of ∇B drift direction are now more carefully investigated. Since some characteristic properties of the L–H transition (e.g. fast time scale and hysterisis) are not explained by the present simulations a discussion of the completing turbulence theories [14–20] is added to Discussion.

The paper is organised as follows. First, we present the applied numerical model and some numerical tests to validate the model. In Sections 3 and 4, E_r profiles are simulated as a function of various parameters and compared to the critical shear for strong turbulence suppression. In Section 5, the effect of reversing the magnetic field on the E_r profile is studied. Section 6 looks at the effect of gradients, and conclusions are drawn in Section 7.

2 Numerical model

The radial electric field on a magnetic surface, $E_r = -(d\Phi(\rho)/d\rho)\langle|\nabla\rho|\rangle$, is solved from the radial current balance, $\langle j_r\rangle = 0$, for the radial current density j_r (quasineutrality condition) neglecting the turbulent electromagnetic field. This corresponds to resolving the gyrokinetic Poisson relation in the limit of $\mathbf{k} = 0$, where $\mathbf{k}$ is the wave vector. Here, $\langle ...\rangle$ denotes the flux surface average, Φ is the electrostatic poten-

tial and ρ is the flux surface coordinate. Although the anomalous *transport* clearly dominates in present tokamak experiments, the anomalous *current* component due to non-ambipolarity in the case of electrostatic fluctuations is relatively small [21]. Here, all the turbulence is neglected except the geodesic acoustic modes [22] included in the electrostatic model. Simulation is done in a real tokamak divertor geometry and the current components are calculated as a time and ensemble average of the guiding centre motion of the test particles in the presence of Coulomb collisions. The radial flux arising from ion-electron collisions is not considered because it causes only ambipolar diffusion which does not affect the radial current balance. The radial current density is therefore

$$j_r(\rho,\theta) = j_{NC} + j_{visc} + j_{pol}, \tag{1}$$

where the terms on the right-hand side correspond, respectively, to neoclassical radial ion current (arising from standard guiding-center drifts and ion-ion collisions), gyroviscosity current, and polarization current. Here, θ is the poloidal angle. In the simulation, the current j_{visc}, which is not a genuine guiding-center drift, and j_{pol}, written here separately from the standard neoclassical current, can be generated by assigning, locally, each ion the following radial drifts (keeping θ and toroidal angle intact during the corresponding drift step) [23]

$$\begin{aligned} v_{visc} &= -(\eta/\Omega B)[\partial^2 E_r(\rho,\theta)/\partial\rho^2]|\nabla\rho|^2, & (2)\\ v_{pol} &= (1/\Omega B)\partial E_r(\rho,\theta)/\partial t. & (3) \end{aligned}$$

Here, $\Omega = eB/m$ is the cyclotron frequency of an ion with charge e and mass m, and B is the magnetic field calculated locally at (ρ,θ). The perpendicular (gyro)viscosity coefficient is given by [24] $\eta = \eta_{Br} \equiv (3/10)k_B T\nu_{ii}/m\Omega^2$, and the ion-ion collision frequency is $\nu_{ii} = e^4 \ln\Lambda n/(4\pi\epsilon_0^2 m^2 v_T^3)$, where $\ln\Lambda$ is the Coulomb logarithm, ϵ_0 is the vacuum permittivity, $v_T = \sqrt{2k_B T/m}$ is the thermal velocity at temperature T, and n is the density of the ions. It should be noted that the gyroviscosity is here treated only in an order-of-magnitude sense and rigorous evaluation of it would require resolving the gyromotion which would make the simulations extremely heavy. However, gyroviscosity is a small contribution and has effect only in high shear regions.

For an ion ensemble, the polarization current can be written as $\langle j_{pol}\rangle = \alpha(\rho)\partial\langle E_r(\rho,\theta)\rangle/\partial t$, where

$$\alpha(\rho) = e\sum_i \frac{|\nabla\rho|(\rho_i,\theta_i)}{\Omega(\rho_i,\theta_i)B(\rho_i,\theta_i)}\frac{p_i}{\langle|\nabla\rho|\rangle}\frac{1}{dV(\rho)} \tag{4}$$

and $\sum_i$ denotes the sum over all ions i in the ensemble with positions ρ_i, θ_i within the flux surface volume element dV at ρ. p_i is the weight factor equal to the total number of ions in a real configuration represented by the ith test particle. Thus, assuming quasineutrality, E_r can be solved from the equation

$$\partial E_r/\partial t = -(1/\alpha)\langle j_{NC} + j_{visc}\rangle \tag{5}$$

on flux surface ρ at time t. This equation is valid for all collisionality regimes. The neoclassical enhancements, related to the inertia in poloidal rotation [25], are hidden

in their complete form in j_{NC}, and do not appear explicitly in the currents $\langle j_{visc} \rangle$ and $\langle j_{pol} \rangle$. The steady-state is found by extending the calculation of the Eq. (5) over several bounce and collision times. In order to do this, the ion radial current, $\langle j_{NC} + j_{visc} \rangle$, has to be evaluated. This can be accomplished by accumulating the net radial ion motion in test particle simulations. We have implemented our method into the five-dimensional Monte Carlo particle-following code ASCOT (Accelerated Simulation of Charged Particle Orbits in a Tokamak) [26]. In ASCOT, each particle is followed along its guiding-center orbit determined by the $\mathbf{E}_r \times \mathbf{B}$ (poloidal or parallel electric field component are not included), gradient- and curvature drifts, collisions, polarization- and gyroviscosity drifts. The particle following takes place in a realistic geometry (including the region outside the separatrix) as shown in Fig. 1 for ASDEX Upgrade and JET. In the ASCOT code the guiding center equations are written in straight magnetic field line coordinates [27] using canonical Hamiltonian variables to avoid numerical drifts. Outside the separatrix where the magnetic field lines are not closed, Cartesian coordinate system is applied. The magnetic background is assumed stationary. When simulating evolution of E_r on a time scale that is fast compared to the evolution of the background by particle transport, electrons can be assumed to provide a stationary neutralizing background, and are not simulated.

For the radial electric field, well-known neoclassical analytical ambipolar value $E_a(\rho)$ (for parallel rotation $U_\parallel \approx 0$) [28] is used as the initial condition. The initialisation of the ion ensemble is done according to the assumed background density and temperature. The test particles are distributed uniformly in radius, and in poloidal and toroidal angle. The weight factors assigned to test particles are proportional to the total number of particles contained in the corresponding volumes, and thus reflect the density profile. In velocity space the particles are distributed evenly in the particle pitch $v_\parallel/v$, and randomly in speed according to a Maxwellian distribution that corresponds to the local temperature. Here, $v_\parallel$ is the parallel component of the total speed v. When a fixed neutralizing electron background is assumed, the radial ion density profile remains practically unchanged, provided that E_r is evaluated from Eq. (5).

Since the radial electric fields related to L-H transition have a radial extent of only a few centimeters an entire plasma cross section is not needed to investigate the relevant physics. Therefore, the computational effort is reduced enormously by restricting the simulation to a relevant region $\rho_L < \rho < \rho_s$ in minor radius. Here, ρ_L is the lower boundary of the simulation regime and ρ_s is ρ at the separatrix. The neoclassical ambipolar E_r [28] is used as the boundary condition at $\rho = \rho_L$ and, at the separatrix, $E_r(\rho_s) = 0$ is adopted. Since the boundary condition may affect the E_r profile inside the separatrix through the gyroviscosity, the value of E_r at the outer boundary is here varied in a large range to show that the chosen value does not have significant effect on the results. In Fig. 2(a), the simulation is done with boundary conditions $E_r(\rho \geq \rho_s) = +20$, 0 and -40 kV/m, and it is shown that the E_r profile is affected only within $\Delta\rho \approx 0.003$, which is, less than 2 mm inside the separatrix. Here, and later in this paper, E_r shown in the figures is the flux surface averaged value. Since we are interested of the shear values in a regime wide enough to suppress the turbulence (≈ 1 cm), the chosen value for $E_{r,edge} = E_r(\rho \geq \rho_s)$ does not affect the conclusions. However, if the viscosity is anomalous, the effect of the boundary condition extends further inside.

The ions hitting the divertor or wall are promptly reinitialized at the separatrix. The reinitialization is uniform in pitch and poloidal angle, with the local Maxwellian velocity distribution. This reinitialization does not create any unphysical current in the simulation domain and, being more uniform (in phase space) than the loss process, it simulates well the replacement of charge lost through the separatrix. In Fig. 2(b), we study the effect of possible poloidal asymmetry in particle source with

two extreme cases where reinitialisition is done to the outboard equator ($\theta = 0$), at the top of the plasma ($\theta = \pi/2$) and at the bottom ($\theta = -\pi/2$). The results are compared to the uniform reinitialisation and comparison shows that in the case with the reinitialisation angle $\theta = \pi/2$ the result indeed somewhat differs from the uniform reinitialisation within some millimeters inside the separatrix but it is plausible that the reality is much closer to the uniform case. When the uniform case is compared to replacement at $\theta = 0$ and $\theta = -\pi/2$, difference is smaller, i.e., if the lost ions in reality are for some reason replaced by ions preferably at the outboard equator or at the bottom, which is, near the divertor target where the main sink of the particles is, uniform reinitialisation still gives a satisfactory approximation for the shear.

In order to properly treat the momentum equation and momentum generation, a binary collision model [29] that conserves momentum and energy in pairwise collisions between the ions has been implemented in the ASCOT code. In the poloidal plane the simulation region is divided into small cells in which particles are randomly paired, and small angle collisions are performed pairwise. The adopted collision operator conserves the number of particles, the total momentum, and the total energy quasi-locally. The model has been recently tested [30, 31] by calculating poloidal rotation relaxation rates for a homogeneous plasma, and by comparing the perpendicular conductivity and parallel viscosity evaluated by ASCOT with the analytical expressions [9, 32]. The simulations were carried out for a wide range of collisionalities and rotation velocities. The binary collision model is used as a default in ASCOT but also option for collisions with fixed background [26] is included for benchmarking and some special purposes. In the present problem, there are reasons not to use the binary collision model in longer runs since the aim is to obtain the result for a given temperature profile. When using the energy conserving collision operator the plasma would indeed cool all the time since the lost particles, which are mainly energetic, are replaced by thermal particles. Thus, to maintain the experimental radial temperature, we rather heat the plasma with the test particle collision operator which assumes fixed Maxwellian background. In Ref. [31] it was shown that both collision models give the same ion flux when a time-independent E_r is externally applied, as long as $U_\parallel$ remains small. Here, parallel rotation starts to develop in the momentum conserving case and the radial flux of ions decays, which is not the case without momentum conservation. However, when E_r is allowed to develop, this takes place faster than the changes in $U_\parallel$ and, because of torque for poloidal rotation posed by orbit loss, enhanced poloidal rotation without significant $U_\parallel$ generation can be sustained. Thus, one may assume that for the same initial $U_\parallel$ one finds the same collisional bulk viscosity contribution and, thus, also the same steady-state E_r for both collision models. In order to show this, the simulations of E_r from Eq. (5) with the two different collision models are compared in Fig. 2(c). It is shown that the lower boundary ρ_L of the simulation regime disturbs the results within $\Delta\rho \approx 0.005$ with both collision operators and, indeed, the disturbance is larger with the binary collision operator. When presenting the results, this regime is excluded from the figures. Further away from the inner boundary and at the outer boundary the results agree.

We emphasize that simulation is not restricted by the assumption of standard neoclassical theory that the orbit width is small compared to the gradient scale length and, we do not have to make artificial assumptions to separate the orbit loss current from neoclassical bulk viscosity current, which has been done earlier both in analytic theory [9] and numerical simulation [33]. The model includes all the effects of neoclassical theory (except the electron diffusion), such as inertia, terms of the nonlinear drift-kinetic equation, convection and corrections due to large poloidal Mach number $M_p = E_r/B_p v_T$. Here, B_p is the poloidal magnetic field. By default, the ripple diffusion is included in the simulation but results presented in this paper are obtained in axisymmetric magnetic configuration. In any case, its effect would

be weak in both devices considered here.

A more detailed description of the method is given in Ref. [34].

3 E_r profile as a function of various parameters

In Ref. [13], E_r profiles have been simulated as a function of mass number A, toroidal magnetic field B_t, temperature T and density n for the ASDEX Upgrade configuration. Here, the same simulation is repeated for JET using discharge #49511 (deuterium plasma) data at the time of the transition, and the results are compared to the ASDEX Upgrade results. JET has a minor radius $a \approx 1$ m, major radius $R = 3$ m, elongation 1.6, plasma current $I = 2.5$ MA, and $B_t = -2.55$ T. Here, the ∇B drift is in the favourable direction, towards the divertor plates. The separatrix density (at $\rho = 1$) in the reference case (referred to as 'BASE' in the figures) is $n_s = 1.4 \times 10^{19}$ m^{-3} and the temperature $T_s = 315$ eV, with the gradient scale lengths $L_n = |n/n'| = 0.205$ and $L_T = |T/T'| = 0.09$ where the prime denotes derivative with respect to radius and is measured at the outboard equator. The numerical value of E_r (and r) at the outboard equator is found using $d\rho/dr = 0.87$ m^{-1}. All the parameters and the corresponding values for ASDEX Upgrade discharge #8044 data are gathered to table 1. Errors in the measurements of density and temperature can be tens of percents.

Fig. 3(a) shows the steady-state profiles of $-d\Phi/d\rho$ for JET in the region $0.97 < \rho < 1$ for a case with plasmas consisting of various hydrogen isotopes and also, in one case, of artificial particles with the same charge number ($Z = 1$) but with mass $A = 10$, in order to more clearly see the mass effect. A difference in the curves can only be seen in about a one centimeter wide regime inside the separatrix. Further inside the results are the same. For hydrogen one obtains a narrow and deep E_r structure which widens and becomes lower as a function of increasing mass number. As discussed in [35], the width of the E_r structure is extended to Min(r_p, L_r) where the poloidal Larmor radius is $r_p = v_T m/eB_p$ which in this case at the outboard equator gives $r_p \approx A^{1/2} 0.5$ cm. Here, $L_r = v_r/\nu_{ii}$ is the radial mean free path based on Coulomb collisions and v_r is the radial drift velocity of the ion. Since $v_r \propto T/ZBR$ we obtain $L_r \propto T^{5/2} A^{1/2}/Z^5 nBR$ for the radial mean free path. For inner plasma radii, $|r - a| > 1 - 3$ cm, where the ion orbit losses become insignificant, E_r is at its neoclassical ambipolar level (determined by $U_\parallel = 0$), which is plotted in Fig. 3(b). In Fig. 3(b)-(d) the steady-state $-d\Phi/d\rho$ profiles are shown for deuterium plasmas for cases where the toroidal magnetic field, temperature and density profiles are changed by scaling the values of the reference case by a constant factor, respectively. Similarly as for ASDEX Upgrade, also here we find a clear effect only when changing the temperature, which is shown in Fig. 3(c). The $E \times B$ shear increases approximately linearly as a function of temperature if the gradient length is kept constant. When comparing Figs. 3(b) and (d), it can be seen that changing the toroidal magnetic field and density gives a qualitatively similar small effect near the separatrix and almost no effect at all at the inner plasma. Any bifurcative solutions predicted earlier in analytic theory [9] were not found here. In these simulations, $L_r \gg r_p$ (except in the lowest T cases) and, thus, E_r structure is determined by r_p. At the ASDEX Upgrade case, L_r and r_p are of the same order. However, if the impurities are taken into account, L_r may dominate in both cases since L_r strongly decreases as a function of Z. Also, for helium L_r is smaller and higher edge T is required to obtain the same shear in $E_r \times B$ flow.

Although the shear due to standard neoclassical effects increases as a function of temperature, it explains only small part of the increase observed here. Major part

of the increase comes from the ion orbit loss effect. When T increases, the orbit width grows, mean free path of the particles increases since ν_{ii} decreases, and radial drift velocity also increases. All these effects increase the ion orbit loss expecially just inside the separatrix. In standard neoclassical theory, the neoclassical return ion flux arising from guiding-centre drifts in the presence of Coulomb collisions (but excluding ion orbit losses) under certain simplifications has an expression [32] $\Gamma_{ret} = -nD[n'/n + \gamma T'/T - e(E_r - B_p U_\parallel)/T] \exp(-M_p^2)$ and is thus an increasing function of E_r for $M_p < 1$. Here, diffusion coefficient D and coefficient γ both depend on collisionality regime. This means that increasing the ion orbit loss requires higher return ion flux, i.e., higher E_r, in order to get the current balance. When going further in, ion orbit loss flux decreases fast (dependence $\exp[-(r-a)^2/r_p^2]$ is given in Ref. [11]) and thus the effect on E_r decreases strongly as a function of radius causing radial gradient in E_r. The absence of bifurcation in the numerical simulations gives support to models [11, 35, 36] in which ion orbit loss current is assumed to have similar dependence on E_r as the neoclassical return current, e.g., $\exp(-M_p^2)$ rather than the almost constant loss current which was assumed in Ref. [9] for $|M_p| < 1$. Similar strong dependence on T and weak dependence on A, n and B_t as was found here has also been predicted with the semianalytical analysis in a circular geometry in Ref. [35] in which the above analytic expression for Γ_{ret} was used and the ion orbit loss current was estimated by numerically integrating the radial drift velocity of the ions which are lost in the divertor along its uncollided orbit within a certain fraction of the collisional mean free path. Thus, the semianalytical approach is at least qualitatively validated by the fully kinetic 5D simulations presented here and, as discussed in Ref. [35], major source of the shear originates from the ion orbit loss current which is a strong function of plasma temperature and distance from the separatrix.

4 Comparison to critical shear

The leading paradigm for the reduction of turbulent transport in H–mode edge plasma is based on sheared radial electric field. The shear in E_r can reduce transport through stabilization of linear modes [37] or by reducing turbulence amplitudes or correlation lengths, or by changing phases between turbulent fluctuations [1]. From Ref. [38] we obtain

$$\omega_{E\times B} = \frac{(RB_p)^2}{B}\frac{\partial^2\Phi}{\partial\psi^2} = \frac{(RB_p)^2}{B}\left(\frac{\partial}{\partial\psi}\right)\frac{E_r}{RB_p} \tag{6}$$

for the $E \times B$ shearing rate. Here, ψ is the poloidal flux. Eq. (6) gives significantly higher shear at the low field side of the tokamak, which is consistent with the fact that the changes taking place inside the separatrix at the L–H transition are often initiated at the outboard midplane [3]. Thus, the shear values obtained from the simulation are also analysed at the outboard equator. In a series of ASCOT simulations, the plasma temperature, density, toroidal magnetic field, and the plasma current have been varied over a wide parameter range of ASDEX Upgrade and JET data. For the parametric dependence of the E_r-shear for ASDEX Upgrade we obtain

$$\omega_{E\times B} \;\propto\; T^{1.06} n^{0.06} B_t^{-0.81} \;[s^{-1}]$$

and for JET

$$\omega_{E\times B} \;\propto\; T^{1.2} n^{0.26} B_t^{-0.89} \;[s^{-1}]$$

with a ± 0.25 error margin in the exponents. I or q_{95} values were not varied enough to make conclusions. For JET, most of the simulations were done in Mark IIGB divertor configuration.

The recently-obtained experimental scaling of the critical temperature for L–H transition in ASDEX Upgrade is [39]

$$T_{cr}(keV) = 0.145 n^{-0.3} |B_t|^{0.8} I^{0.5}. \tag{7}$$

Here, T_{cr} and n are evaluated at $r = a - 2$ cm, n is expressed in 10^{19} m^{-3}, B_t in Teslas and I in mega-amperes. In JET, an unconstrained fit to experimental data gives [40]

$$T_{e,top}(keV) = 0.39[0.19, 0.81] n_{ea}^{-0.64\pm0.15} B_t^{1.69\pm0.18} A_{eff}^{-0.15\pm0.19} q_{95}^{-0.86\pm0.57} \tag{8}$$

where A_{eff} is the effective mass (in atom mass units), q_{95} the safety factor at ψ_{95}. Again, B_t is given in Teslas and n_{ea} is expressed in 10^{19} m^{-3}. $T_{e,top}$ is the electron temperature at time of L–H transition at the location where the top of the pedestal (measured with the heterodyne radiometer) in H-mode is located [41] and n_{ea} is the line averaged density from the far-infrared (FIR) interferometer at the fixed point $R = 3.75$ m [42]. Since $n(R)$ at the time of transition is rather gently sloping, we can assume that $n_{ea} \approx n_{95}$ holds. When comparing this scaling to the simulation results it is assumed that the top of the temperature pedestal is at ψ_{95}, which is roughly the case in ELM-free (Edge Localized Mode) H–mode [43]. In the absence of realiable data for edge ion temperature, $T_i \approx T_e$ is assumed which has also been measured in experiments using charge-exchange diagnostics of edge T_i for NBI (Neutral Beam Injection) heated discharges [42]. By comparing Eqs. (7) and (8), one notices that for typical parameters of these two tokamaks, the transition temperature is essentially higher for JET than for ASDEX Upgrade. However, since $q_{95} \propto B_t/I$ the parametric dependence of the threshold temperature in these two devices is somewhat similar, although the error bars are large. As the multi-machine database [44] gives dependence $T_{crit} \propto R^{0.93}$ for the L–H transition threshold temperature, most of the difference between the two devices can be explained by the different major radius. The dependence on major radius may arise, for example, due to mean free path that decreases as a function of R and thus higher T is required to obtain wide enough high shear region for strong turbulence suppression. Larger major radius also decreases ion orbit loss current which depends on radial drift velocity $v_r \propto T/R$.

In order to compare the level of the obtained shear values to the experimental scaling of the L–H transition, a criterion for low and high shear values corresponding to L and H mode is needed. In Figs. 4(a) and (b) we compare the ASDEX Upgrade simulations to the scaling of Eq. (7) and the shear values of JET simulations to the scaling of Eq. (8), respectively. Here, an *ad hoc* criterion for the critical shear $\omega_{E\times B}$ is chosen separately for ASDEX Upgrade and for JET to get the best fit between the numerical and experimental results. The chosen criterion has to be fulfilled at least over a turbulence decorrelation length from the separatrix. In ASDEX Upgrade case the criterion 5×10^5 s^{-1}, and in the JET case the criterion 1.5×10^5 s^{-1}, gives the best fit. This can be compared to the BDT (Biglari-Diamond-Terry) criterion for the strong suppression of turbulence which is $|\nabla E/B| > \Delta\omega_t/k_\theta \Delta r_t$ [4]. Here, $\Delta\omega_t$ is the turbulent decorrelation frequency, Δr_t is the radial correlation length, and k_θ is the mean poloidal wave number of the turbulence. Typical values of turbulence parameters observed at Doublet-III-D (DIII-D) are $\Delta\omega_t = 2.5 \times 10^5$ s^{-1}, $\Delta r_t = 0.7$ cm^{-1} and $k_\theta = 1$ cm^{-1} [6], which would give a threshold shear of 3.6×10^5 s^{-1}. Similar values for critical shear have also been obtained directly from E_r measurements at

DIII-D and, also, at TEXTOR [5]. Thus, in both cases the criterion is in rough quantitative agreement with the experimental measurements of the critical shear. The question still remains why the critical shear in the JET example seems to be lower than in the ASDEX Upgrade case. The main differences in these two examples are plasma current, threshold temperature and the profile widths at the edge. The critical shear as a function of A, B_t and I has been studied experimentally [7] in limiter device TEXTOR-94 and the dependence

$$\nabla E_{crit} \approx 61 \times B_t^{1.4} A^{-1.2} I^{-1.66} \tag{9}$$

in (kV m^{-2}, T, amu, MA) was found, in which the dependence on I would justify using a lower threshold for JET plasmas than for the ASDEX Upgrade plasmas. In that study, the temperature dependence was not investigated and, also, it is possible that phenomena determining ω_{crit} are different in limiter and divertor devices. If one assumes that the turbulence is due to ion temperature gradient modes, $\omega_{E\times B}$ should exceed the maximum growth rate $\gamma_{max} \sim v_T/(R^\alpha L_T^{1-\alpha})$ [3] $(0 < \alpha < 1)$ in order to stabilize turbulence. Again, in agreement with simulations, lower critical shear for JET is obtained at L–H transition conditions although the threshold temperature is higher than in ASDEX Upgrade.

5 The effect of reversing the magnetic field

In experiments, the threshold power needed for L–H transition is essentially higher when the ∇B drift is away from the X-point (unfavourable direction) than when it is towards it (favourable direction). It has been observed that keeping the heating power and all the other parameters unchanged, the edge profiles of n_e and T_e for normal and for reversed B_t are very similar [45]. Thus, in Fig. 5, the effect of reversing the direction of B_t is studied keeping n and T profiles and all the other parameters fixed. In the ASDEX Upgrade case the edge plasma is in the collisional parameter regime and in the JET case in a collisionless regime. Here, 'normal' refers to the case were the ∇B drift is towards the X-point. The parameters are those given in Sec. 3 for the reference cases. Data for the reversed field case are obtained from the data of the reference cases by simply changing the sign of B_t. In the figures it can be seen that within the limits of accuracy of the simulation, the E_r profiles do not change when B_t is reversed. Thus, the simulations with reversed magnetic field presented here can not explain the difference in L–H transition power threshold unless one assumes that the critical shear is different in the reversed field case.

In the simulations so far, the temperature and density profiles have been modified from the transition condition data by scaling the profiles by a constant factor. In Fig. 6, real experimental density and temperature data across the transition for ASDEX Upgrade discharge #8044 as well as the E_r profiles obtained when using these profiles are shown. For comparison, the same simulation is done for the improved L-mode discharge #8595 in which ∇B has opposite direction, i.e., the unfavourable direction. Simulation with the real profiles is done only for ASDEX Upgrade since for JET no accurate enough measurement of the density and temperature at the edge exists. When comparing the two cases shown here, the density profiles are very similar and do not change considerably as a function of time. However, in both cases the temperature increases due to heating, and for ∇B drift towards the X-point, transition to the H–mode is observed in experiments. Here, however, E_r and its derivative change smoothly on a collisional timescale following the changes in the temperature and density profiles. No indication of bifurcative solutions is found at the time of the transition. In the case where the ∇B drift is away from the X-point, the plasma still remains in L–mode although the temperature at the edge is much

higher than at the L–H transition conditions for the opposite direction. Shear is indeed much higher for this improved L–mode than for the H–mode conditions of discharge #8044.

6 Effect of density and temperature gradients

In the scalings often only the local values of n and T are used, although the gradients of these variables may have as much importance. However, the n and T profiles in the 2–3 cm wide simulation regime are often determined only by two measured values and a constant gradient between these data points is assumed. Thus, the effect of second derivative is neglected. Also, both the location and value of these measured data points is inaccurate, thus making the value of the gradients even less accurate. In addition to the uncertainty in the fine structure of the plasma parameters near the edge, also the statistical error in the radial current determination from finite particle ensemble affects determining the shear at the edge.

In order to study the effect of gradients numerically, we here increase the gradients keeping the values at the separatrix constant. In Fig. 7(a), the reference case and the case with two times higher density are plotted together with the case where the density at the separatrix, $\rho = 1$, is that of the reference case but increases to the value of the high density case (n×2) at $\rho = 0.975$. In Fig. 7(b), the same test is done for the temperature profiles. It can be seen that by increasing the temperature gradient or the density gradient, the level of the E_r profile clearly increases, but the gradient does not. Indeed, for the temperature, increasing the derivative gives almost zero E_r gradient near the edge. These results, however, must not be generalised since dependence of E_r on T' (and n') may vary in different collisionality regimes. In order to test if the gradient lengths can explain part of the differences in JET and ASDEX Upgrade results, in Fig. 7(c) a test is done where we keep the separatrix densities and temperatures as well as all the other parameters fixed, but use the L_n and L_T of our ASDEX Upgrade reference data in the JET discharge and vice versa. Results show that the shear in E_r does not change much when the gradients are changed although the E_r level changes. In standard neoclassical theory, in the absence of ion orbit losses, the shear in E_r depends strongly on L_n and L_T, but this is a small contribution when compared to the shear due to ion orbit loss effect, which, based on these results, is not sensitive to the gradients.

7 Discussion and conclusions

Although the rapid transition from low to high confinement is well documented experimentally and the important role of E_r shear in turbulence suppression is recognized, the mechanism by which the radial electric field is formed in the transition is still unclear. Here we have shown that, for experimental plasma conditions near an L-H transition, the high $E \times B$ shear relevant for turbulence suppression can be generated by neoclassical effects together with ion orbit losses. The highest shear region in the simulation seems to be of the order of poloidal Larmor radius in agreement with some experimental results, but also further in it can be above the threshold. However, the results given here do not explain hysteresis and the effect of the direction of the ∇B drift on the power threshold. Since in experiments, for a given heating power, the density and temperature profiles are similar for both directions of B_t and since in the simulations E_r profile does not change when B_t is reversed, the critical shear for strong turbulence suppression should be different

when B_t is reversed, in order to match the simulation results to the experimental findings.

In investigating the criterion for the high shear matching simulations to the experimental results, we noted that the shear needed in JET is lower than in ASDEX Upgrade. Thus, if the simulation presented here includes the most important physics affecting the shear, then the critical shear should be somewhat higher in ASDEX Upgrade conditions at least when these two typical examples are considered. This is consistent with the experimental observations and theoretical models in which the critical shear decreases as a function of R, L_T or I. The fast time scale of the transition observed in some experiments is not explained by the present simulations since E_r in the model follows the changes in local density and temperature which take place on a collisional time scale. Any bifurcative solutions predicted earlier in analytic theory [9] were not found here. Thus, our simulation is in agreement with the experimental data which suggests that the transition is continuous process (see Ref. [46]) and, if a bifurcative process is needed to explain experiments, it is likely to come from turbulence theory rather than from neoclassical current balance. Some of the assumptions in analytic theory have been tested numerically for the ion orbit loss [33] and the neoclassical return current [31]. Since quite a good agreement between analytic theory and numerical simulation was found for the neoclassical return current in Ref. [31], it might be that the ion orbit loss current is the one which fails more as a function of E_r thus causing bifurcation in analytic theory [9] in which the loss current is almost constant for $M_p \leq 1$. However, since the ion orbit loss current and the neoclassical return current consist of same current carriers, and since the separation of these two is impossible in practice, it was necessary to perform a self-consistent test particle simulation of the edge plasma in which both of these effects (and some more) were included in the particle motion.

While the present fully kinetic 5D simulation undoubtedly captures the most salient features of the neoclassical physics with finite orbits and allowance for large Mach rotation and while it makes an important step in incorporation of the boundary effects for the edge equilibrium, there are at least three important simplifications in the adopted model: First, the scrape-off layer plasma has not been simulated, and thus, secondly, the replacement of the lost ions by true sources like gas puffing and recycling has not been modeled from first principles, and thirdly, the boundary condition for E_r at the separatrix has been arbitrarily set. However, as shown in Sec. 2, E_r profile inside the separatrix is affected by the boundary value only on a regime which is not significant when the suppression of turbulence is considered. Also, tests with different reinitialization schemes indicate that the shear in E_r inside the separatrix by orbit loss to large extent can be evaluated without extending the calculation of the source of return current to the scrape-off layer. However, the poloidal distribution of this source has been found to affect the results, and thus in future work a more detailed comparison with experiments should be done, e.g., for the neutral distribution around the separatrix for the experimental conditions. Poloidal dependence of the plasma density and temperature (as well as momentum) profile and neutrals outside the separatrix may have some effect (to large extent by collisions) on ion orbit loss rate, but this is not investigated here. It should be added here that comparison of the divertor heat load profile on the divertor plates as calculated from the present model with the load profile at JET observed by thermocouples has shown similar features, in particular for the width and asymmetry of the high heat load peak next to the separatrix [47] giving credibility to the orbit loss model in the present paper. Also, consistent with some recent experiments, simulations with the present model indicate higher power threshold for helium plasmas [13], but further investigation of this is left for future work.

One important simplification in our model is the neglect of anomalous current components. If the turbulence is electromagnetic, it is possible that the anomalous

fluctuations contribute to the current balance since drift-wave magnetics are different for ions and electrons [48]. An L–H transition model based on this effect [19] predicts, however, positive E_r near the edge in contradiction with experiments. Also, experimental evidence favours electrostatic turbulence [49]. Although the anomalous current itself can often be assumed ambipolar, the anomalous convection may have a non-ambipolar secondary effect since it may affect the loss cone population and thus influence the non-ambipolar ion orbit loss current. Neglect of this may be a significant simplification in the current model, but inclusion of the effect is far beyond the scope of this paper.

One candidate for the instability responsible for the L–mode anomalous transport is the ion temperature gradient (ITG) driven mode. In Ref [20], the sheared slab simulations showed that the anomalous viscosity increases with $\omega_{E\times B}$ to some critical value beyond which it falls leading to L–H transition in the model. To reach this critical value, some driving mechanism is needed which can be, e.g., the ion orbit losses. In Monte Carlo simulations of Ref. [35], anomalous enhancement of gyroviscosity is shown to decrease the level of $\omega_{E\times B}$, but there the effect is not dramatic. However, it is possible that ITG turbulence is already suppressed at the time of transition by some other mechanism. This can be, for example, the time-dependent zonal flows, which have been neglected in this paper. The zonal flows, which have radial and temporal scales comparable to those of the turbulence, have been shown to reduce turbulence to a lower level without fully quenching it [15, 18]. Thus, it is possible that the fast time-scale changes observed in L–H transition are due to self-generated zonal flows, and the rest of the turbulence is suppressed by the mean E_r shear from neoclassical equilibrium. Turbulence-driven flows and sudden transition to reduced transport have also been observed in fluid [16] and gyrokinetic [17] turbulence simulations by varying the pressure gradient. In Ref. [17], fast changes due to self-generated zonal flows were observed, and inclusion of E_r from neoclassical equilibrium in the model had a further stabilizing but more gradual effect. A realistic geometry with the scrape-off layer has been considered in Ref. [14] by solving fluid equations including self-consistent profile evolution together with turbulence. In this model, turbulence-generated flow shear stabilizes high toroidal mode number modes causing transition if the power is increased enough. To conclude, although the neoclassical equilibrium E_r can not explain the fast time scale of the L–H transition, it may have an important role in transition dynamics both by determining the rough parametric dependence of the transition threshold and by further improving the confinement after the transition. Turbulence theory, however, is needed to explain the details of the transition itself.

Acknowledgements

Dr. Parail and Dr. Fundamenski are acknowledged for useful discussions. This work benefited from the computing resources of Centre of Scientific Computing in Finland.

References

[1] Terry P W 2000 *Reviews of Modern Physics* **72** 109

[2] Burrell K H 1997 *Phys. Plasmas* **4** 1499

[3] Connor J W and Wilson H R 2000 *Plasma Phys. Control. Fusion* **42** R1

[4] Biglari H, Diamond P H and Terry P W 1990 *Phys. Fluids* **B2** 1

[5] Jachmich S *et al* 1998 *Plasma Phys. Control. Fusion* **40** 1105

[6] Gohil P, Burrell K H and Carlstrom T N 1998 *Nucl. Fusion* **38** 93

[7] Jachmich S and Weynants R R 2000 *Plasma Phys. Control. Fusion* **42** A147

[8] Itoh K and Itoh S-I 1996 *Plasma Phys. Control. Fusion* **38** 1

[9] Shaing K C and Crume E C Jr 1989 *Phys. Rev. Lett.* **63** 2369

[10] Kim J *et al* 1994 *Phys. Rev. Lett.* **72** 2199

[11] Fukuyama A *et al* 1994 *Plasma Phys. Control. Fusion* **36** A159

[12] Fukuyama A *et al* 1996 *Plasma Phys. Control. Fusion* **38** 1319

[13] Heikkinen J A, Kiviniemi T P and Peeters A G 2000 *Phys.Rev.Lett.* **84** 487

[14] Xu X Q *et al* 2000 *Phys. Plasmas* **7** 1951

[15] Hahm T S *et al* 1999 *Phys. Plasmas* **6** 922

[16] Rogers B N *et al* 1998 *Phys. Rev. Lett.* **81** 4396

[17] Parker S E *et al* 1999 *Phys. Plasmas* **6** 1709

[18] Scott B *et al* The influence of zonal $E \times B$ flows on edge turbulence in tokamaks and stellarators *Nucl. Fusion* submitted

[19] Itoh S-I and Itoh K 1988 *Phys. Rev. Lett.* **60** 2276

[20] Staebler G M, Dominguez R R, 1993 *Nucl. Fusion* **33** 77

[21] Stringer T E 1992 *Nucl. Fusion* **32** 1421

[22] S.V. Novakovskii *et al* 1997 *Phys. Plasmas* **4** 4272

[23] Spitzer L 1962 *Physics of Fully Ionized Gases*, 2nd Ed., Interscience Publishers, New York; Eq. 2.42.

[24] Braginskii S I 1965 *Reviews of Plasma Physics* (Consultants Bureau, New York) Vol.1.

[25] Novakovskii S V *et al* 1995 *Phys. Plasmas* **2** 3566

[26] Heikkinen J A and Sipilä S K 1995 *Phys. Plasmas* **2** 3724

[27] White R B and Boozer A H 1995 *Phys. Plasmas* **2** 2915

[28] Hinton F L and Hazeltine R D 1976 *Rev. Mod. Phys.* **48** 239

[29] Ma S, Sydora R D Dawson J M 1993 *Comput. Phys. Commun.* **77** 190

[30] Kiviniemi T P, Heikkinen J A and Peeters A G 2000 *Phys. Plasmas* **7** 5255

[31] Kiviniemi T P, Heikkinen J A and Peeters A G 2000 *Nucl. Fusion* **40** 1587

[32] Stringer T 1993 *Nucl. Fusion* **33** 1249

[33] Heikkinen J A *et al* 1998 *Plasma Phys. Control. Fusion* **40** 693

[34] Heikkinen J A, Kiviniemi T P, Kurki-Suonio T, Peeters A G and Sipilä S K Particle Simulation of the Neoclassical Plasmas *Journal of Computational Physics* submitted

[35] Heikkinen J A, Kiviniemi T P and Peeters A G 2000 *Contrib. Plasma Phys.* **40** 431

[36] Itoh S I and Itoh K 1989 *Nucl. Fusion* **29** 1031

[37] Lehnert B 1966 *Phys.Fluids* **9** 1367

[38] Hahm T S and Burrell K H 1995 Phys. Plasmas **2** 1648

[39] Suttrop W *et al* 1997 *Plasma Phys. Contr. Fusion* **39** 2051

[40] Righi E *et al* 2000 *Plasma Phys. Control. Fusion* **42** A199

[41] Righi E *et al* 1999 *Nucl. Fusion* **39** 309

[42] Ryter F, H Mode database working group 1996 *Nucl. Fusion* **36** 1217

[43] Breger P *et al* 1998 *Plasma Phys. Control. Fusion* **40** 347

[44] Snipes J A and the International H–mode Threshold Database Working Group, 2000 *Plasma Phys. Control. Fusion* **42** A299

[45] Carlstrom T N *et al* 1999 *Nucl. Fusion* **39** 1941

[46] Hugill J 2000 *Plasma Phys. Control. Fusion* **42** R75

[47] Matthews G *et al* Divertor Energy Distribution in JET H–modes *Journal of Nuclear Materials* to be published

[48] Callen J D, 1977 *Phys. Rev. Lett.* **39** 1540

[49] Endler M *et al*, 1995 *Nucl. Fusion* **35** 1307

Tables

Table 1. Reference parameters for ASDEX Upgrade (AUG) and JET.

case	a(m)	R(m)	B_t(T)	I(MA)	L_n(m)	L_T(m)	n_s(m^{-3})	T_s(eV)	$\nabla\rho$(m^{-1})
AUG	0.5	1.65	-2.5	1	0.023	0.026	1.2e19	120	1.73
JET	1	3	-2.56	2.5	0.205	0.09	1.4e19	315	0.87

Figure Captions

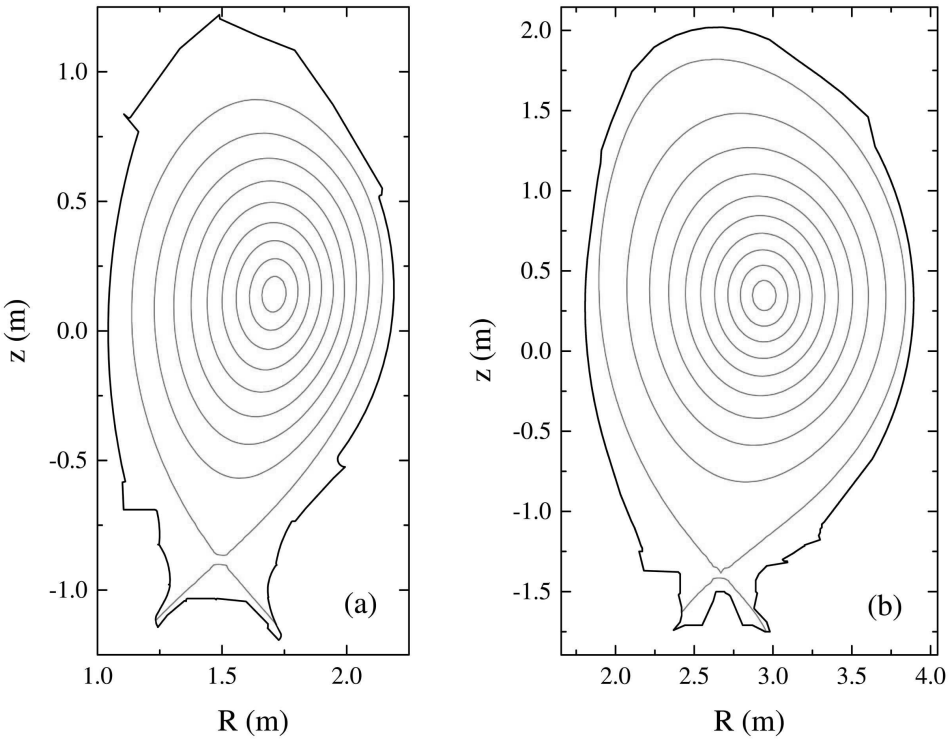

Figure 1: *Real magnetic field background data, including wall and divertor structures, from experimental data bases of a) ASDEX Upgrade, and b) JET is used in the simulations.*

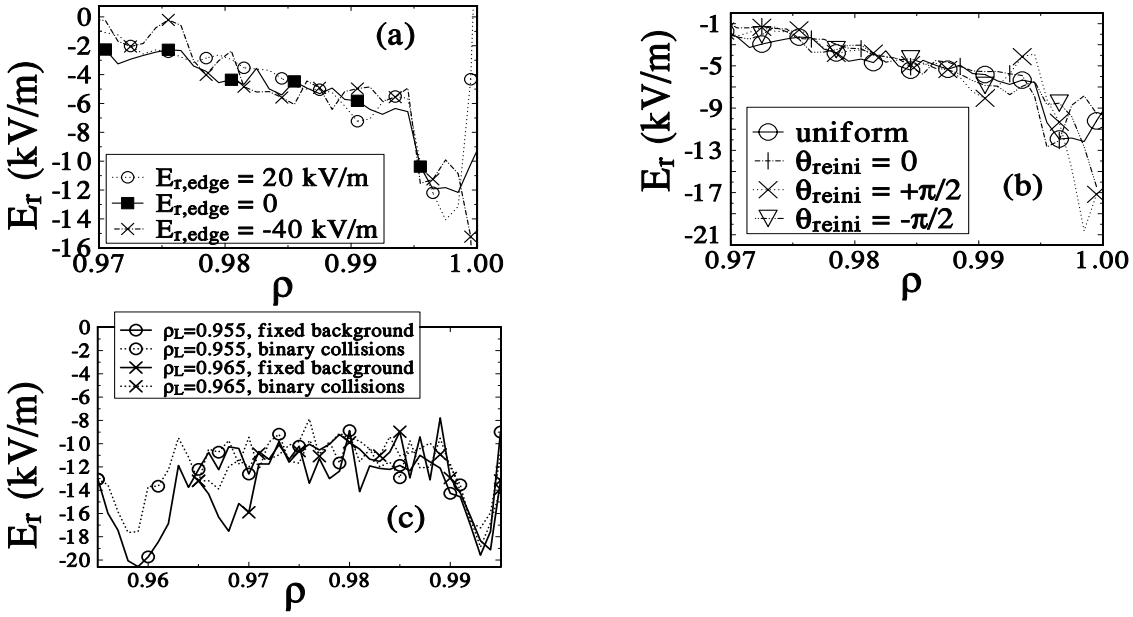

Figure 2: *(a) Effect of boundary condition, (b) effect of reinitialisation, (c) momentum conserving vs. fixed background collision operator and the effect of lower boundary ρ_L of the simulation regime. In these tests, ASDEX Upgrade parameters are used.*

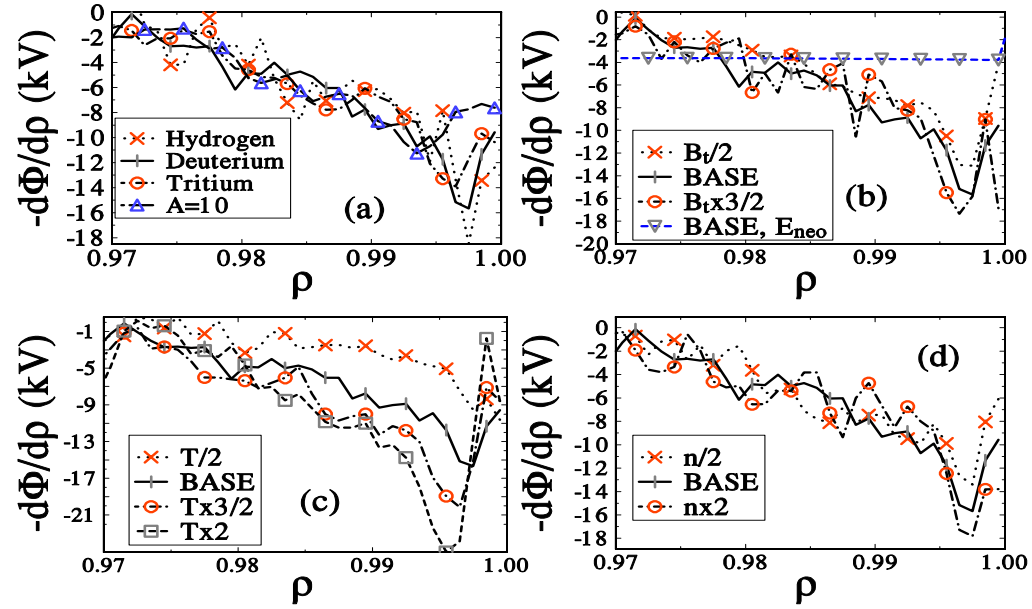

Figure 3: *$-d\Phi/d\rho$ as a function of radius for various plasma (a) isotope, (b) magnetic field, (c) temperature and (d) density, where 'BASE' refers to the JET L–H transition conditions. In (b) also the neoclassical ambipolar level (for $U_{||} \approx 0$) from analytic theory is shown for the reference case.*

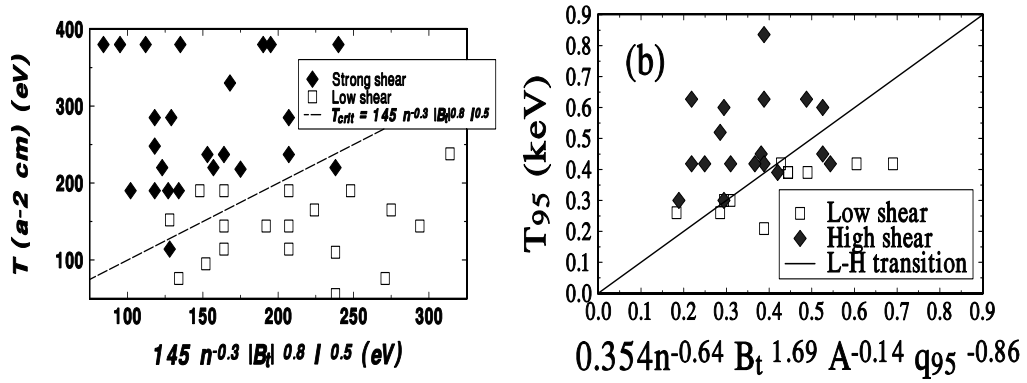

Figure 4: *Shear values of $E \times B$ flow from ASCOT simulation as a function of experimental parametrisation of critical temperature of L–H transition for (a) ASDEX Upgrade and (b) JET. Experimental critical temperature is shown as a straight line in the figure.*

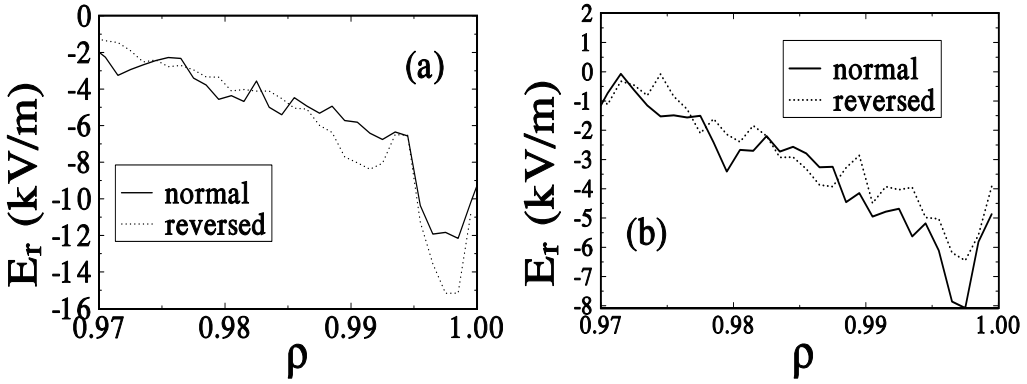

Figure 5: *Effect of reversing the direction of magnetic field at (a) ASDEX Upgrade and (b) JET is minimal if all the other parameters are kept fixed.*

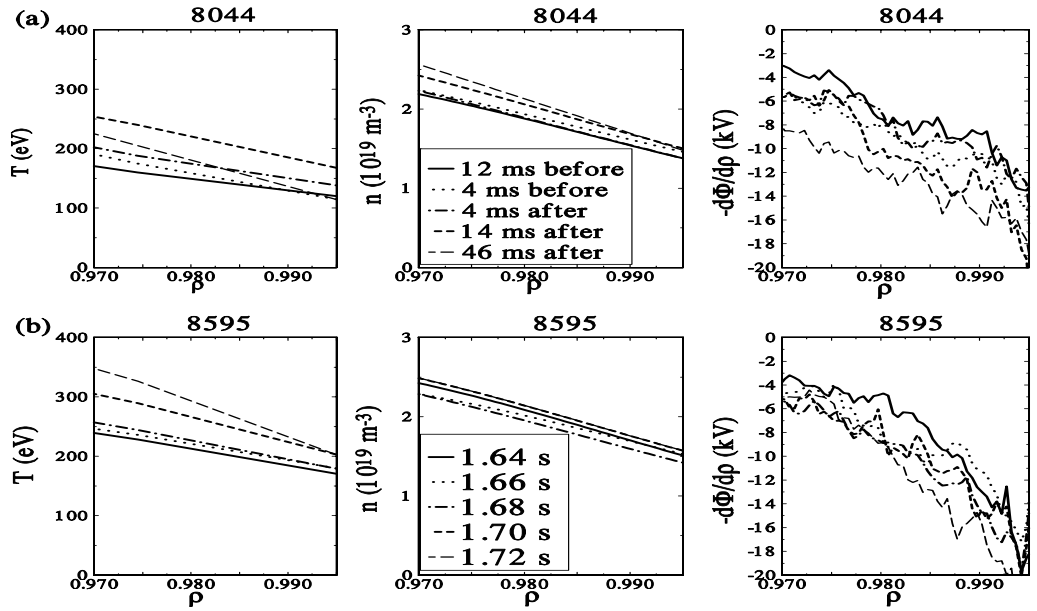

Figure 6: $-d\Phi/d\rho$ *as a function of radius using experimental density and temperature data (a) across the transition in ASDEX Upgrade (#8044) and (b) for the improved L-mode discharge (#8595). Note that the shear is higher in the latter case although it is in L–mode.*

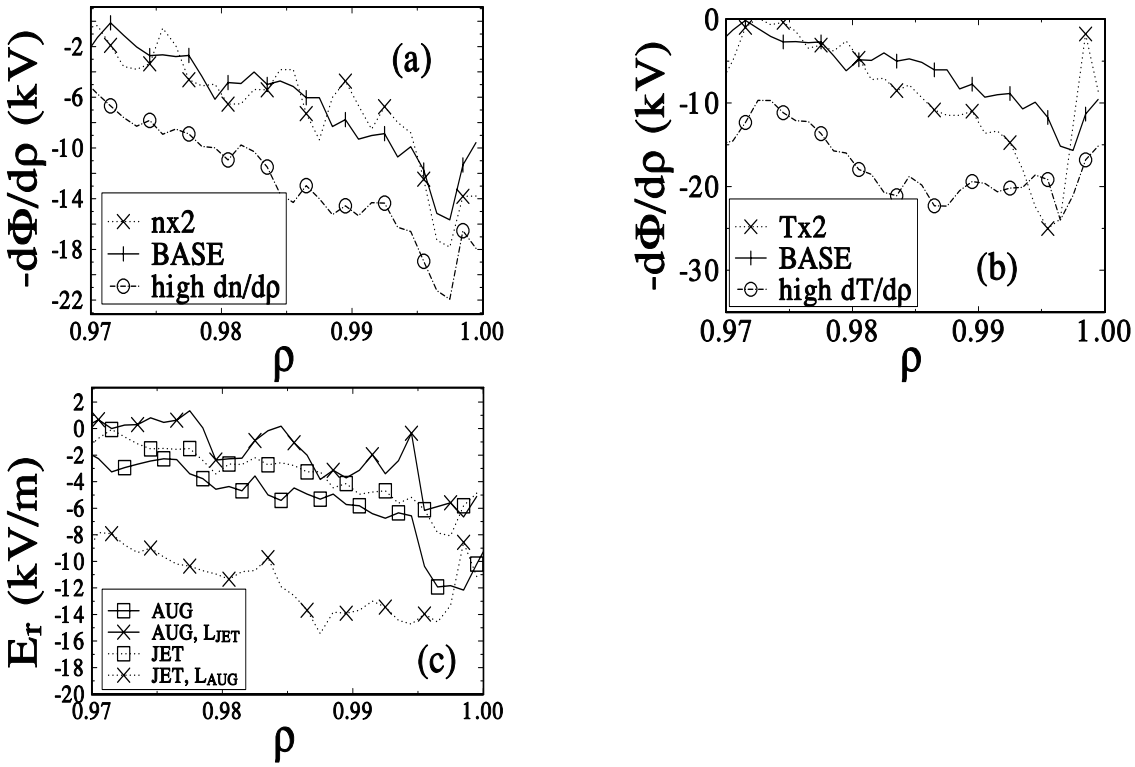

Figure 7: *Effect of (a) density and (b) temperature gradient, and (c) changing the gradient lengths on the shear values.*